A Self-Adaptive High/Low Beam Spotlight Filter in Capturing Local Structure Information for Object Contour Extraction

Roy Chaoming Hsu *rchsu@mail.ncyu.edu.tw*
Electrical Engineering Dept.
National Chiayi University
Chiayi City, 600355, Taiwan

Chia Hung Hsu *billy.hsu@atenlab.com.tw*
Atenlab, Neihui District
Taipei City, Post code, Taiwan

Abstract

Contour extraction is a method in exactly obtaining an object's contour from images. It is considered as one of the most important pre-processing for image processing applications. In this study, a self-adaptive high/low beam spotlight filter (SAHLBSF) is designed to capture local structure information for object contour extraction. The proposed SAHLBSF is inspired from the users' experiences in car driving, where when the road is very straight and clear, a low beam light is applied, while a high beam light will be utilized when the road is winding and/or the environment is dark. Utilizing the SAHLBSF, the local structural information between two pre-selected initial contour points are captured and the candidate contour points are then determined. The spotlight filter continues for all pairs of initial points of an object such that a broadband of the object's contour is constructed. A thinning process is then applied to obtain the final one-pixel-wide exact object contour. Experimental results using artificial and real medical images showed that better contour extraction performance can be obtained the proposed SAHLBSF than other existing methods.

Keywords: Contour Extraction, Local Structure Information, Spotlight Filter.

1. INTRODUCTION

Image processing technique has been commonly used in many fields, such as medical image processing and recognition(Ruhaiyem & Hammade, 2021; Sanya et al., 2021,; Bakir&Charfi,2009;Barat & Lagadec, 2008),robot vision (Zhanget at., 2019), and industrial inspection (Weimer et al., 2016) , etc… Before conducting image processing for specific image applications, the original image often requires certain pre-processing, such as image enhancement (Yan & Kassim, 2006, Yang et al., 2010), de-noising (Talukder et al., 2018), or smoothing in obtaining an improved quality of image for the following processing and applications. Image segmentation (Chen et al., 2010, Qiao et al., 2019) is considered as one of the most important pre-processing for specific image applications. Because the accuracy of the segmentation might have strong influence for the following image processing applications, hence, how to increase the accuracy of the image segmentation is the most crucial work in image processing.

Edge detection and contour extraction are the most important steps in image segmentation. Method for edge detection could be categorized into gradient-based (Canny, 1986), region-based (Hojjatoleslami & Kittler,1998) and model-based (Kass, et al., 1989; Liu & Sclaroff, 2004) method according to the characteristic of processing. Contour extraction technique has been considered as another form of edge detection with closed contour for an object in a region of interest and is often applied in medical image processing (Suzuki et al., 2004; Xu, et al., 2016; Zhang et al., 2016) and robot vision(Zhang et at., 2019). The accuracy of determining object contour from

region of interest is very important in medical image processing because it affects the following surgical diagnosis and/or treatment. In robotic application, a robot often uses vision system in identifying object contour, which recognition requires accurately calculation and delineation of object contour using machine vision, such that the robot can further perform certain tasks, such as grasping the object with the robot arm.Recent literatures focus on applying deep learning to the contour extraction of medical images and show significant resultsin the area of tongue contour extraction(Zhu et al. 2019;HamedMozaffari& Lee, 2019; Jaumard-Hakounet al., 2016).However, in most of the deep learning based contour extraction methods, manual labeling, initialization, monitoring, and manipulation are frequently required. In this study, a self-adaptive high/low beam spotlight filter (SAHLBSF) is designed to capture local structure information for object contour extraction without the computationally expensive of neural network training. The details of the proposed SAHLBSF and the experimental results are described in the following.

2. METHODOLOGY

The overall process flow of the proposed SAHLBSF for contour extractionis shown in Figure 1,where the initial boundary points on the object contour is first automatically selected by the Initial Inflection Contour Points Detection method (IICPD) (Hsu et al., 2011) and segments with nearly straight line between two initial points are generated. Secondly, the pairs of initial contour points are provided as input to the SAHLBSF for extracting possible object contour points. Thirdly, to avoid disconnected contour segments from the step 2, the dilation process is performed to form a closed wideband of object contour. Finally, a thinning method (Guo & Hall, 1989) is performed to generate a one-pixel-width object contour. After performing the IICPD in the first step of Figure 1, pairs of initial contour points can be connected to form the normal direction of the defined spotlight filter. The proposed AHLBSLF then will be applied for each pair of neighboring initial contour points. The detailed processing flow of the proposed SAHLBSF for object contour extraction is shown in Figure 2.

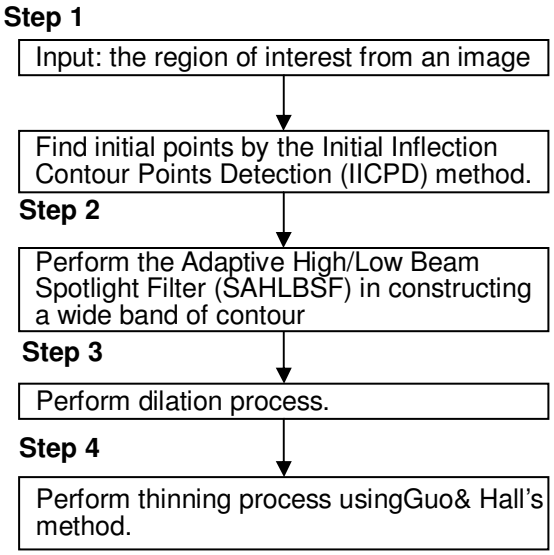

FIGURE 1: Flowchart of the proposed SAHLBSF for object contour extraction.

In the step 1 of Figure2, the parameters of high beam spotlight and low beam spotlight, respectively, are defined by (r_h, θ_h) and (r_l, θ_l), where the $r$and θ, respectively, are the radius and spanning angle of a spotlight. The region of interest (ROI) image, f(*x*,*y*), and a set of initial contour points, $P_i, i = 1 \ldots N$ obtained by performing the IICPD are provided as the input to the AHLBSLF. An edge strength map, R(*x*,*y*), is defined as the collection of evidence for contour and the pixels of the R(*x*,*y*) are initialized to 0. Figure3 shows the schematic diagram of the high beam and low beam spotlight sectors, represented by $S_h(r_h, \theta_h)$ and $S_l(r_l, \theta_l)$, respectively. The spotlight's

normal direction is constructed by connecting the starting contour point $p_i(x_i, y_i)$to the terminal contour point$p_{i+1}(x_{i+1}, y_{i+1})$. In order to allow each spotlight to have the same amount of pixels, each spotlight in Figure3 should have the same area as

$$A = \frac{\theta_h \times r_h^2}{2} \cong \frac{\theta_l \times r_l^2}{2} \quad (1)$$

where A is the area covered by both high beam and low beam spotlight sector. Hence, the relationship of θ and$r$ between high beam and low beam spotlight isas the following.

$$\frac{\theta_h}{\theta_l} = \frac{r_l^2}{r_h^2} \quad (2)$$

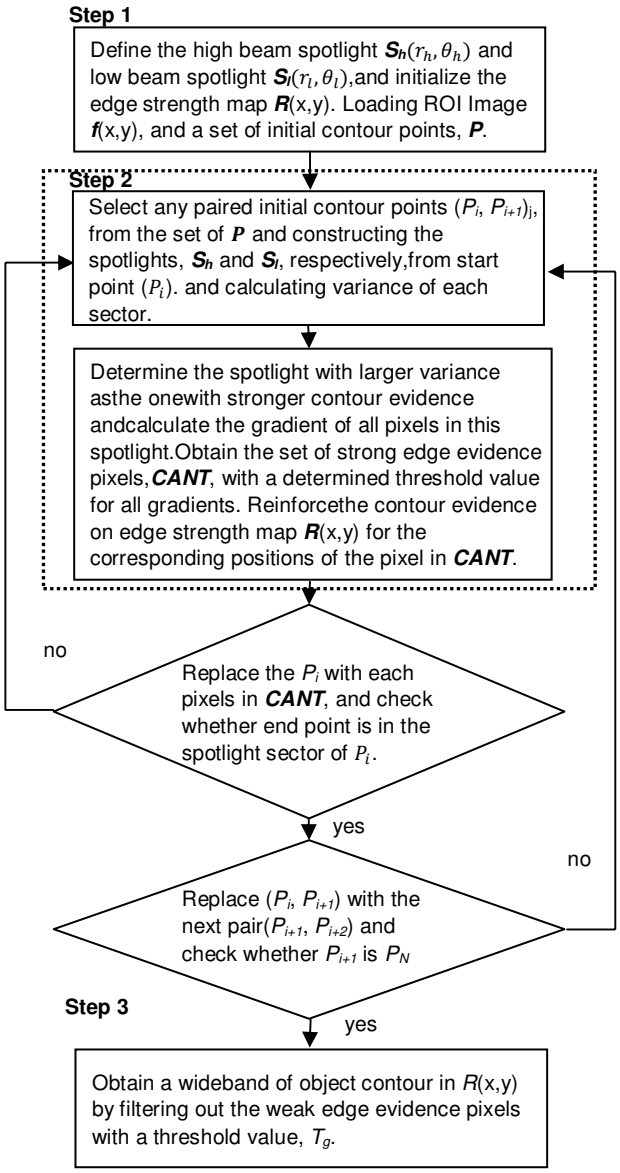

FIGURE2: The main processing flow of SAHLBSF.

In the step 2 of Figure2, a pair of initial contour point P_i and P_{i+1} are selected as starting and terminal point, respectively. Then the spotlights can be constructed by connectingP_i, the origin of

the spotlights, and the terminal point P_{i+1}, as the normal direction, $\boldsymbol{D_i}$, of the spotlight and expanding θ, the spotlight angle. The local structure information of the image area covered by the spotlight spotlights, i.e. the mean and variance, are then calculated by the following equations

$$\mu_{S_h} = \frac{1}{N_h}\sum_{i=1}^{N_h} f(x,y) \tag{3}$$

$$\mu_{S_l} = \frac{1}{N_l}\sum_{i=1}^{N_l} f(x,y) \tag{4}$$

and

$$\sigma_{S_h}{}^2 = \frac{1}{N_h}\sum_{i=1}^{N_h}(f(x,y) - \mu_{S_h})^2 \tag{5}$$

$$\sigma_{S_l}{}^2 = \frac{1}{N_l}\sum_{i=1}^{N_l}(f(x,y) - \mu_{S_l})^2 \tag{6}$$

where $N_h$and$N_l$are the total number of pixels in the S_h and S_l, respectively. $f(x,y)$ is the intensity of each image point at position (x,y).

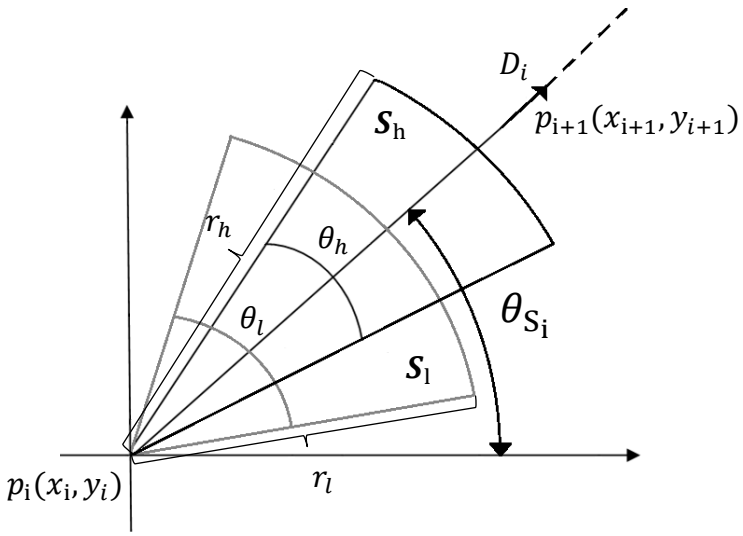

FIGURE3: The geographical definition of the spotlight sectors.

The variances of pixels covers by the S_h andS_l are compared, where spotlight sector with larger variance indicates the contour most likely lay inside this spotlight covered area. The gradients of the pixels covered by the spotlight sector with larger variance are then computed and compared with a gradient threshold, r_T, which is calculated by the accumulating histogram of all gradient valuesin the region. The pixels withgradient larger than $r_T$are considered as possible contour candidates and are collected to form a contour candidate set ***CANT***. A reinforcing process of adding numbers on edge strength map ***R***(x,y) for the corresponding positions of the pixel in ***CANT*** is performed. After the reinforcing process, each pixel in the ***CANT***is considered as the starting point of P_i and the operation of local structure information captured by spotlight repeats until the last initial contour point pair (P_i, P_{i+1}) is processed and the edge strength map $R(x,y)$ is finally constructed, wherethe pixel value of $R(x,y)$ represents how strong the edge evidence is for the same position of pixel in image $f(x,y)$.In step 3, a filtering process with the threshold value $T_g$is performed on edge strength map $R(x,y)$ to delete pixels with low evidence of contour point. Such filtering operation leaves the pixels with stronger edge evidence in the edge strength map and finally forms a wide band of object contour. The proposed contour extraction then goes to the

step 3 of dilation process and step 4 (Guo & Hall, 1989) of Figure1 to finally construct a one-pixel-width object contour as mentioned in the beginning of this section.

3. PEROFORMANCE EVALUATION METRICS AND DATA SET

3.1 Performance Evaluation Metrics

In this experiments, artificial images and real medical images have been used to illustrate the effectiveness of the proposed SAHLBSF contour extraction methodof this study. In the experiment of artificial images, white Gaussian noise is added to simulate the situation of images with noiseand the signal to noise ratio (SNR)is calculated, as follows, in dB to show the strength of the signal.

$$\mathrm{SNR} = 10 \times \log_{10}\left[\frac{\sum_{x=1}^{N_x}\sum_{y=1}^{N_y}(f(x,y))^2}{\sum_{x=1}^{N_x}\sum_{y=1}^{N_y}(f(x,y)-\hat{f}(x,y))^2}\right] \tag{7}$$

In (7), the numerator is the image signal value of the original picture, and the denominator is the difference between the original picture and the picture after adding noise, which can be called the size of the noise. The numerator is a fixed term, so when the noise is added, the greater the denominatoris, thelower SNR value will be, indicating that the image has a high degree of noise and the object contour of the ROI image are possibly harder to detect.To evaluate the performance for artificial image, the accuracy of the contour extraction is defined as the following

$$Accuracy = \frac{accurate\ detected\ contour\ points}{totoal\ detected\ contour\ points} \times 100\% \tag{8}$$

where the denominator is the number of total detected contour points, and the numerator is the number of contour points which are actually detected.

3.2 Data Set

In this experiment, an artificial irregular star-shape image and two real medical images,as show in Figure 4, were selected for testing the SAHLBSF and other existing contour extraction methods.

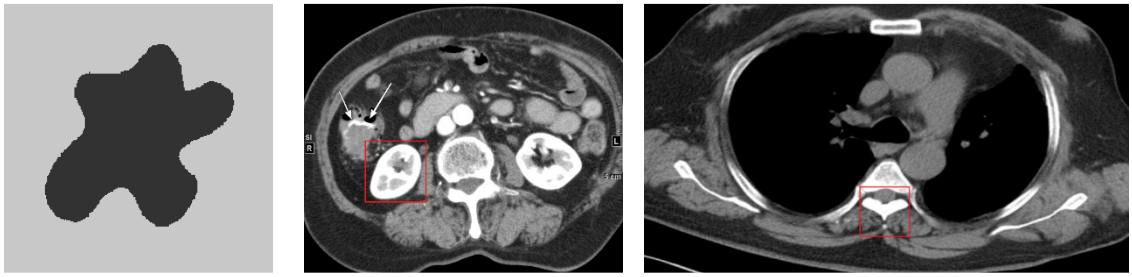

(a) Star-shape artificial image (b) CT image of the diverticulitis (c) CT image of the spine

FIGURE 4: The dataset of the experiment. (a) Star-shape artificial image, (b) CT image of the diverticulitis, and (c) (c) CT image of the spine.

In Figure 4(a), the star-shape artificial image was selected because the ground truth real contour points were known such that the accuracyin (8) can be computed for the performance evaluation. The value of the foreground pixel, i.e., the star-shape, of the original artificial image is 70 and the value of the background pixel is 200. The size of thestar-shape artificial image is 256X256, with 8 bits of greyscale value.To verify the proposed SAHLBSF contour extraction method of this study can also be applied to real medical images, 2 real medical images which are CT image of the diverticulitis and spinewere selected as well,, as shown in Figure 4(b) and 4(c), respectively. The square area marked in redin the medical imagesare the region of interest (ROI) with size of 150X150 and 140X140, respectively for the kidney and the spinethat requires the object contour

extraction.The medical images used in this experiment are from the Cancer Image Archive (TCIA) http://www.cancerimagingarchive.net/ website.

4. EXPERIMENTAL RESULTS

In this study, the resulting images of object contours of the proposedSAHLBSFcontour extraction method were compared and analyzed by comparing with the results of ACM (Kass et al., 1998) method, the basic spotlight filter method (Liu et al., 2012), the tri-directional spotlight filter method (Hsu et al., 2014), the adaptive spotlight filter (Lin, 2013),and the Somkantha method (Somkantha et al., 2011). The ACM method, also called snake, is to obtain the contour of the image byprocessing through a set of initial contour points close to the edge of the object, and the energy formula converges to obtain the contour of the object in an image.The basic spotlight filter method is the most primitive modelof spotlight filter, and the contour is extracted through precise calculation andjudgment of the local structure captured by the spotlight filter around the contour points.The tri-directional spotlight filter method uses a more complex spotlight model to extract contours in three neighboring and overlapping spotlightsectorsbased on the captured local structure within each spotlight sectors.The adaptive spotlight filter method defines the expansion angle of the spotlight through a more complex mathematical model, and then adjusts the radius of corresponding spotlight sector and threshold ratio for contour extraction. The object contour extraction method of Somkantha (Somkantha et al.2011) utilizes the combination of image gradient texture features and gradient strength, and defines the direction of pursuit through a mask to extract object contour.

4.1Experimental Results for the Artificial Images

The experiments for SAHLBSF was first conducted using the star-shape artificial image added with different levels of noise.The noise-added star-shape artificialimages are shown in Figure5(a), 5(b), and 5(c) with SNR of 27.23dB, 24.11dB and 21.65dB, respectively. The initial contour points, obtained by IICPD, marked with white“+”, are shown in Figure5(d), 5(e), and5(f) for the Figure5(a), 5(b) and 5(c), respectively.

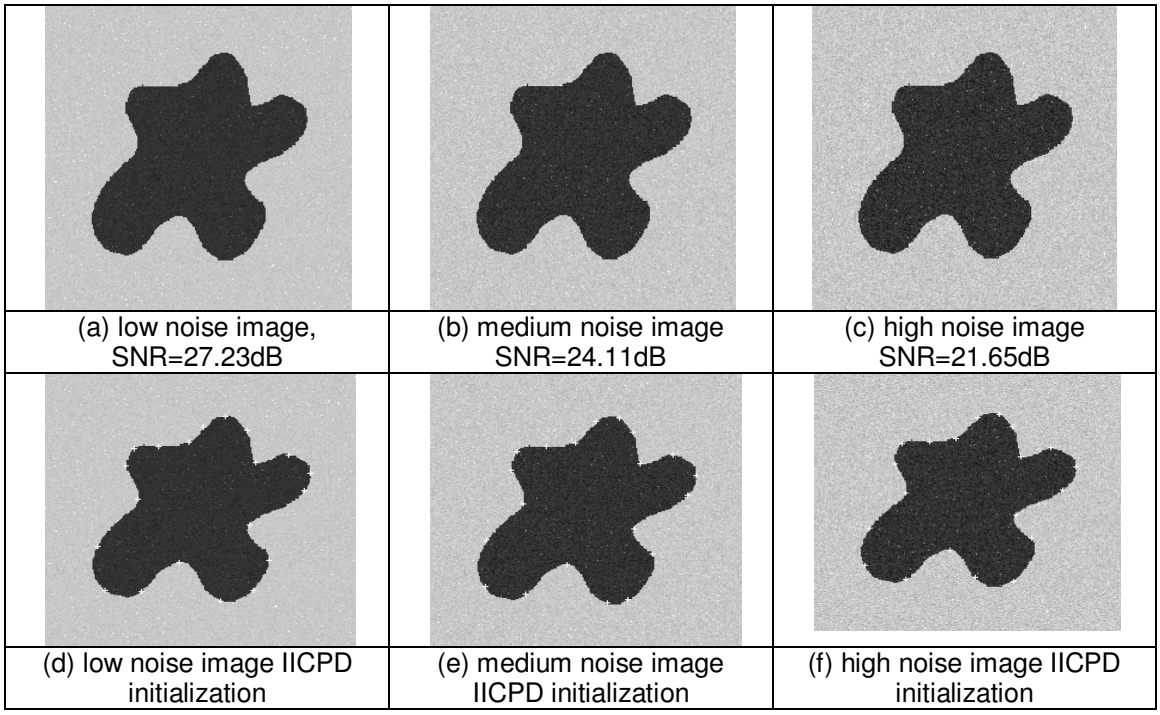

(a) low noise image, SNR=27.23dB	(b) medium noise image SNR=24.11dB	(c) high noise image SNR=21.65dB
(d) low noise image IICPD initialization	(e) medium noise image IICPD initialization	(f) high noise image IICPD initialization

FIGURE 5: The test artificial images with SNR =27.23 dB (a), SNR =24.11 dB (b), SNR 21.65dB (c) and the image with initial points (d), (e) and (f), respectively.

Methodology	Parameters
The proposed SALHBSLF	$S_h(r_h, \theta_h) = (10, {}^{\pi}/_{3})$ $S_l(r_l, \theta_l) = (8, {}^{\pi}/_{2})$
Basic spotlight filter	$S(r, \theta, r_T) = (8, {}^{\pi}/_{3}, 0.6)$
Tri-directional spotlight filter	$S(r, \theta, \Delta\theta, r_T) = (8, {}^{\pi}/_{3}, {}^{\pi}/_{18}, 0.6)$
adaptive spotlight filter	$\Delta = \left\{\frac{5\pi}{18}, \frac{\pi}{3}, \frac{7\pi}{18}, \frac{4\pi}{9}\right\}$
ACM(Snake)	$\alpha = 0.2 \ 、 \ \beta = 0.3 \ 、 \ \gamma = 1$
Somkantha method	$\alpha = 0.2 \ 、 \ \beta = 0.3 \ 、 \ \varepsilon = 1$

TABLE 1: The parameters used by the comparing methods for the object contour extraction.

The resultsof object contour extraction obtained using the proposed SAHLBSF are shown in Figure 6.Figure 6(a), 6(b), and 6(c), respectively, shows the contour extracted by the proposed SAHLBSF for the low, medium, and high level noise star-shape artificial image as shown in Figure 5(a), 5(b), and 5(c) by utilizing the IICPD generated initial contour points. To clearly compare whether the contour is extracted exactly on the edge of the object, the extracted contour is overlaid on the original noisy image, as shown in Figure 6(d), 6(e), and 6(f)and the selected square area in Figure 6(d), 6(e), and 6(f) are magnified, as shown in Figure 6(g), 6(h), and 6(i), respectively. By observing Figure 6(g), 6(h), and 6(i),one can easily find that with such a large curvature changein the selected magnified area, the proposed SAHLBSF method could adaptively select spotlights between the high beam and the low beam to extract the precise contour for the star-shape artificial image with different level of noises.

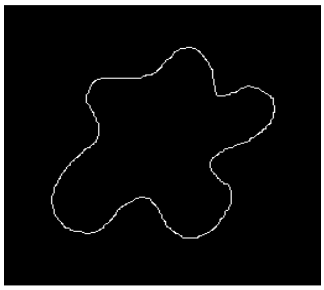

(a) Closed contours of low noise image

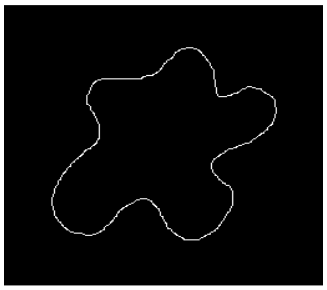

(b) Closed contours of medium noise image

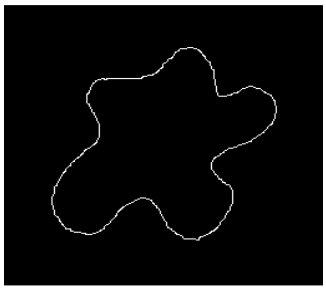

(c) Closed contours of high noise image

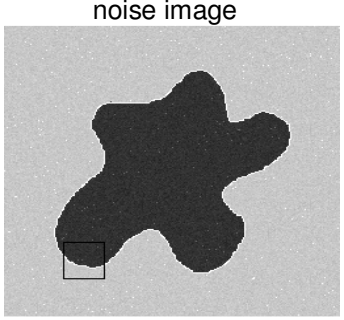

(d) Object contour overlay on lownoise image with selected square area

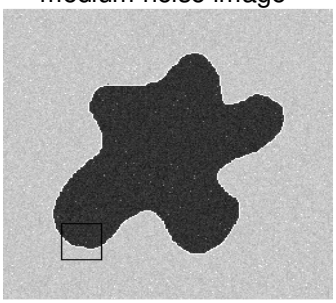

(e) Object contour overlay on medium noise image with selected square area

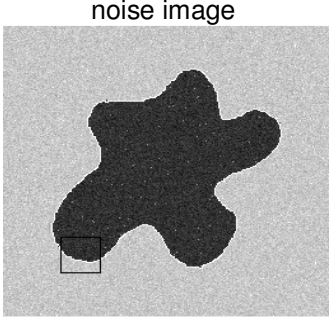

(f) Object contour overlay on high noise image with selected square area

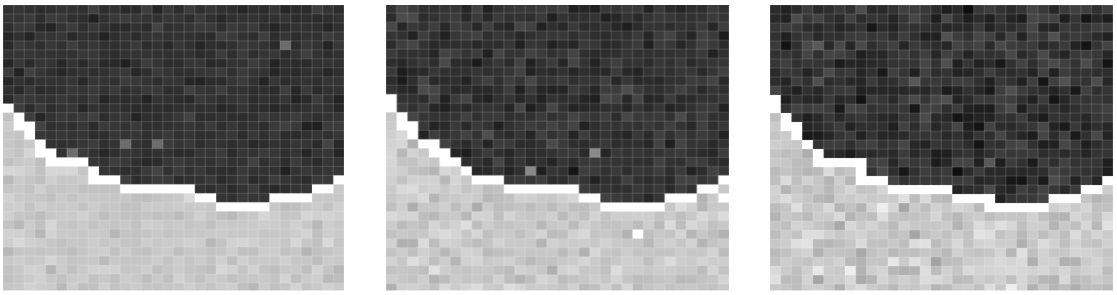

(g) Selected zoom out block for low noise image (h) Selected zoom out block for medium noise image (i) Selected zoom out block for high noise image

FIGURE6: The experimental resultsof the proposed SAHLBSF method for the star-like artificial imageswith three level of noise. (a), (b), and (c), respectively, shows theclosed contours of low, medium, and high noise artificial image. (d), (e), and (f), shows the object contour overlay on low, medium, and high noise image with selected square area. Figure 6(g), (h), (i), respectively shows the magnified area as indicated in Figure 6(d), (e), and (f).

The object contour extraction results of the proposed SAHLBSFmethod for the three different noise level of star-like artificial images are comparing with other existing methods discussed in the beginning of this section. For demonstration purpose, only the experiment results of high noise level star-like artificial image are shown as in the Figure 7. Figure 7(a), (b), (c), (d), (e), (f), respectively, shows the original star-like artificial image with added high level of noise of SNR=21.65dBoverlaid by the object contour extraction results of the proposed SAHLBSF, basic spotlight filter, tri-directional spotlight filter,adaptive spotlight filter, snake, and Somkantha method.

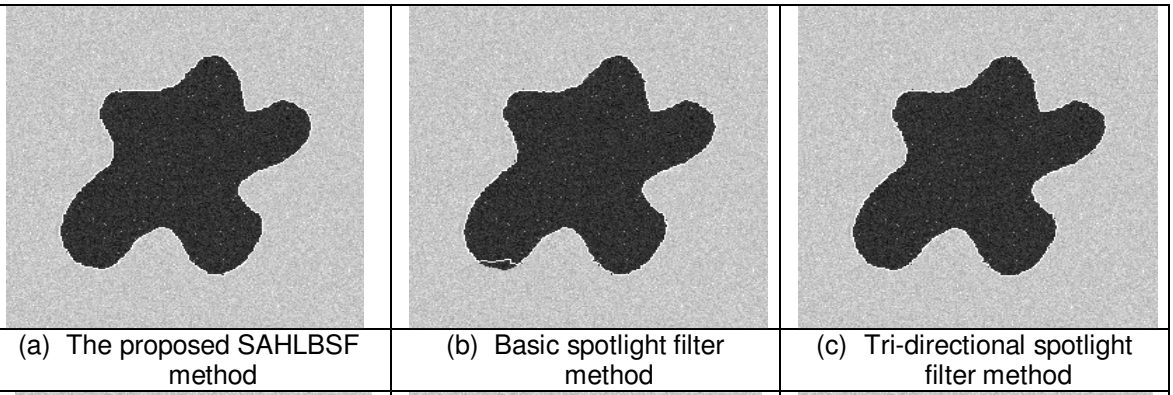

(a) The proposed SAHLBSF method | (b) Basic spotlight filter method | (c) Tri-directional spotlight filter method

(d) Adaptive spotlight filter method | (e) ACM(snake) method | (f) Somkantha et al.method

FIGURE7: Object contour extraction of the star-like artificial images for the comparing methodsof (a) The proposed SAHLBSF method, (b) basic spotlight filter method, (c) tri-directional spotlight filter method, (d) adaptive spotlight filter method, (e) ACM (snake), and (f) Somkantha method for the star-like artificial image with SNR=21.65dB.

Figure 8 shows the magnified object contour extraction resultsof the square area indicated in Figure 6(f) for the comparing methods for the star-like artificial image with SNR=21.65dB. It can be clearly seen that the contour extracted by the proposed SAHLBSF method is quite close to the outline of the object by visual observation of Figure 7(a) and Figure 8(a). In comparing with other methods, one can see that the extracted contour of the proposed SAHLBSF method is precisely and perfectly matched to the edge of the artificial noisy star-like image of Figure5(c). By observing the contour extracted by the basic spotlight filter method in Figure 7(b), it is found that the real edge is not fully extracted whichcauses the entire contour to deviatein the magnified area, and finally a significant error value occurred, as shown in Figure 8(b). The contour extraction results of tri-directional and adaptive spotlight filter method have the similar extracted contour matching to the ground truth with that of the proposed SAHLBSF method by visual inspection of the Figure 7(c) and Figure 8(c), and Figure 7(d) and Figure 8(d). On the snakeresults, one can be seen that the contour deviates slightly inwardas shown in Figure 7(e) and 8(e), which indicated that the snake is unable to extractmany details of contour accurately. Finally, the Somkantha method has the characteristics of searching contour by depending on the gradient strength value of the edge, while the gradient strength value also affects the edge pointsit pursuits, and finally produces a slight error, as shown in Figure 8(f).Performance evaluation of the comparing methods for the star-like artificial image with low, medium, and high level of noise is shown in Table 2. The calculation results of the accuracy of other existing methods shownthat the accuracy of the proposed SAHLBSF methodis superior to the basic spotlight filter, ACM, and Somkantha et al. method, yetslightly better than these of the tri-directional and theadaptive spotlight filter methodsin terms of overall detection accuracy. Because of the dynamic adjustment of the threshold, the proposed SAHLBSF method achieves better matching contour to the ground truth edge outline. In terms of execution efficiency and convenience of parameter setting, the proposed SAHLBSF method uses fewer mask operations, the computational complexity can be better than thoseof the other three spotlight filter based methods. Becausethe proposed SAHLBSF method only needs to define the radius and the expansion angle of high beam and low beam in the parameter setting.

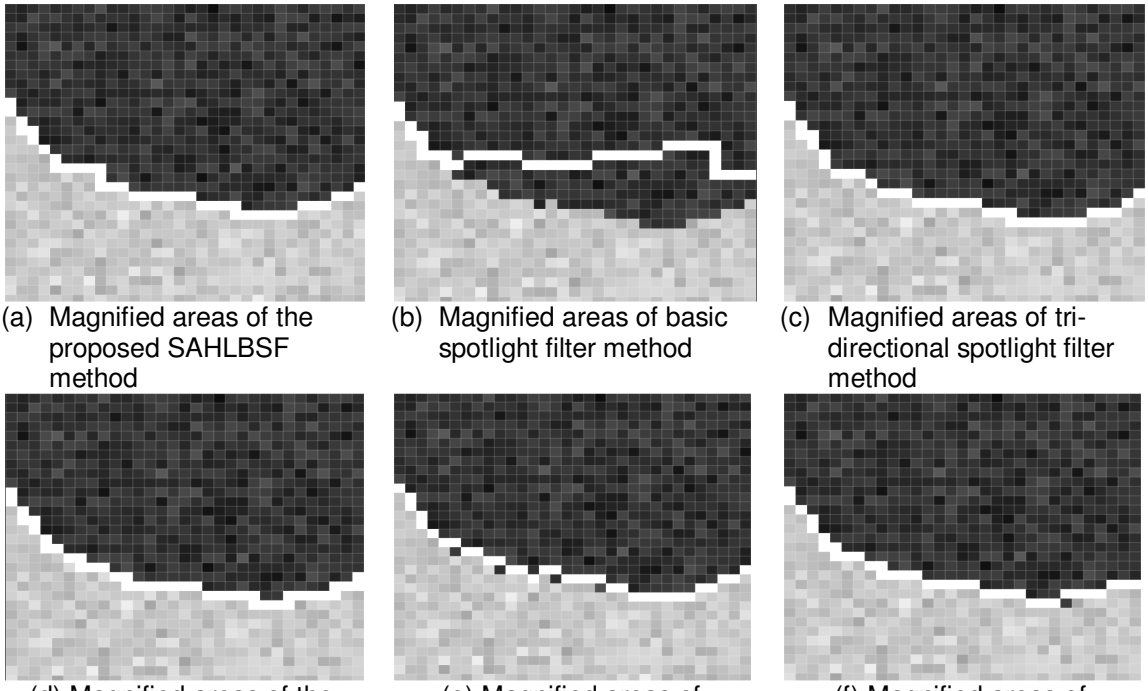

(a) Magnified areas of the proposed SAHLBSF method

(b) Magnified areas of basic spotlight filter method

(c) Magnified areas of tri-directional spotlight filter method

(d) Magnified areas of the adaptive spotlight filter method

(e) Magnified areas of ACM(snake)

(f) Magnified areas of Somkantha et al. method

FIGURE8: The magnified object contour extraction result of the square area indicated in Figure 6(f) for the comparing methods for the artificial noisystar-likeimage with SNR=21.65dB.

SNR / Method	27.23 dB, low noise	24.11dB, medium noise	21.65dB, high noise
the proposed SAHLBSF	100 %	99.55 %	99.25 %
Basic Spotlight Filter	99.09 %	95.22 %	94.38 %
Tri-directional Spotlight Filter	99.85 %	99.12 %	98.54 %
Adaptive Spotlight Filter	99.85 %	99.14 %	98.72 %
ACM(Snake)	92.69 %	92.40 %	92.09 %
Somkantha et al.	99.55 %	98.95 %	97.74 %

TABLE 2: Performance evaluation of the comparing methods for the star-like artificial image with low, medium, and high level of noise.

4.2 Experimental Results for the Medical Images

The ROI images of Figure 4(b) and 4(c) are magnifiedand shown inFigure 9(a), and 9(b), respectively, while the initial contour points generated by the IICPD for Figure 9(a), and 9(b) are shown in Figure 9(c) and 9(d), respectively with a red "+" sign for the contour extraction.

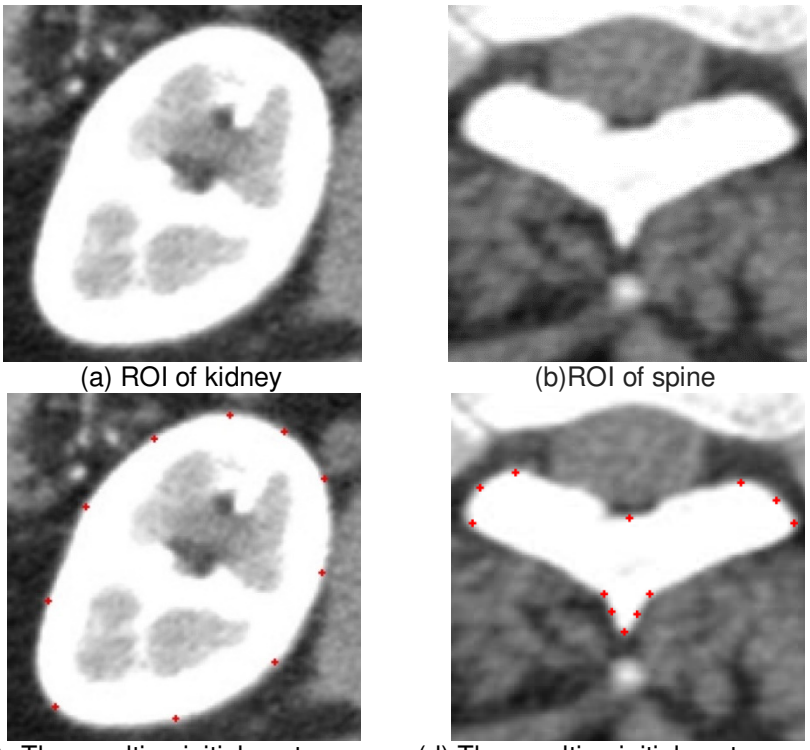

(a) ROI of kidney (b)ROI of spine

(c) The resulting initial contour points by IICPD for the kidney (d) The resulting initial contour points by IICPD for the spine

FIGURE9: The resulting initial contour points for (a) kidney and (b) spine by executing IICPD for the magnified ROI of the real medical images.

The parameters used in the comparing methods for the medical images are listed in Table 3.

Method	Parameters
The proposed SALHBSLF	$S_h(r_h, \theta_h) = (10, {}^{\pi}/_{3})$ $S_l(r_l, \theta_l) = (8, {}^{\pi}/_{2})$
Basic spotlight filter	$S(r, \theta, r_T) = (8, {}^{\pi}/_{3}, 0.6)$
Tri-directional spotlight filter	$S(r, \theta, \Delta\theta, r_T) = (8, {}^{\pi}/_{3}, {}^{\pi}/_{18}, 0.6)$

adaptive spotlight filter	$\Delta=\left\{\frac{5\pi}{18},\frac{\pi}{3},\frac{7\pi}{18},\frac{4\pi}{9}\right\}$
ACM (Snake)	$\alpha=0.2\ 、\ \beta=0.3\ 、\ \gamma=1$
Somkantha et al. method	$\alpha=0.2\ 、\ \beta=0.3\ 、\ \varepsilon=1$

TABLE 3: The parameters used by the comparing object contour extraction methods for the real medical images.

Figure 10shownthe object contour extraction of the kidney image by the comparing methods and the resulting contour extracted by each of the methodis overlaid on the ROI kidney image.By examining Figure 10(a), one can see that the proposedSAHLBSF method can accurately extract the contour of the object in the real medical image. The contour extraction result of the proposed SAHLBSF method isthen compared with the contour extraction results obtained by the basic spotlight filter, tri-directionalspotlight filter, adaptive spotlight filter, snake], and Somkantha et al. method. In observing the resulting object contour extraction of basic spotlight filter method, as in the lower left corner of Figure 10(b), the positionsof extracted contourshift inwards.Because the area between the two initial contour points has a larger curvature, so some of the edgescannot be covered bythesinglespotlight, resulting in poor contour extraction. Figure 10(c) and 10(d) shows the extracting results of the tri-directional spotlight filterand the adaptive spotlight filter, respectively, both spotlight filters results exhibit much better extraction precision than the basic spotlight filter. Because the total spanning areas of tri-directional spotlights and the adaptive spotlight is much wider than the basic spotlight such that the curvature along two initial contour pointscan be covered by both spotlight filters. In the snake, it can be foundfromthe result in Figure 10(e) that the contour can be closely depicted, yet the contour tends to be bounded inward due to the convergence of energysuch that some details may not be fully described. The Somkantha et al. method uses Canny's operator as the basis and combines the texture intensity generated by the Gaussian filter, so it may be subject to the threshold value of the Canny method. Hence, the noise spots left over from the top in Figure 10(f) cause the final inaccuracy in contour detection.

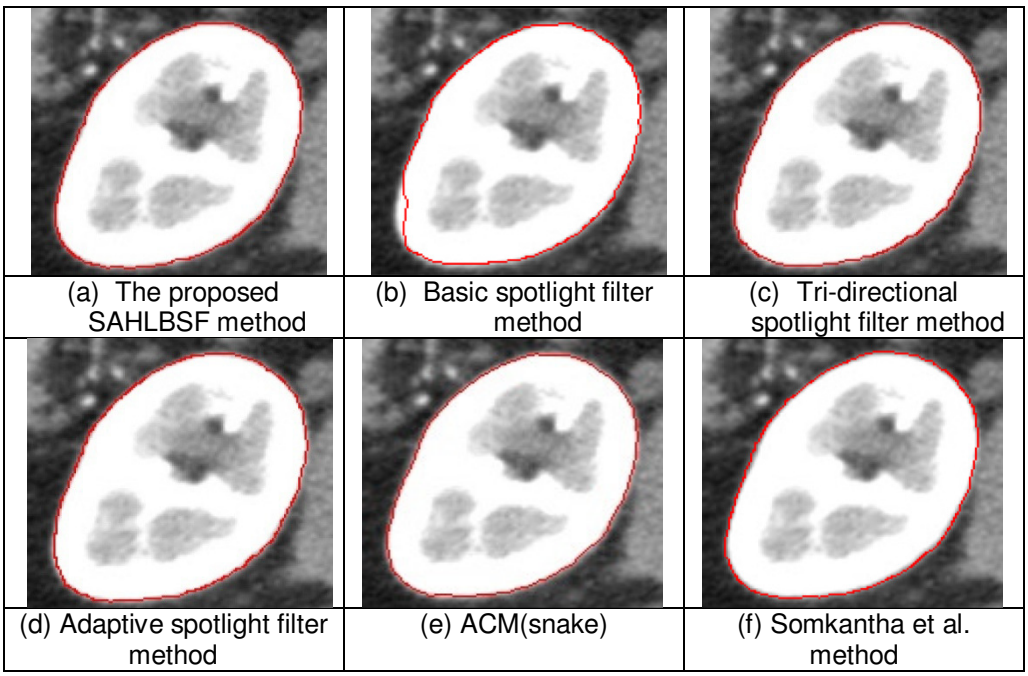

FIGURE 10: Object contour extraction of the kidney by the comparing methods and the contour is overlaid on the kidney image. (a) The proposed SAHLBSF method, (b) basic spotlight filter method, (c) tri-directional spotlight filter method, (d) adaptive spotlight filter method, (e) ACM (snake), and (f) Somkantha et al. method.

To clearly examine the contour extraction results, selected block of the same portion of imagefrom Figure 10is magnified and shown in Figure 11 for all comparing methods.By inspecting the magnified image of Figure 11, it is found that the contour extraction of the proposed SAHLBSF method achieve best fit of the contour in comparing with other existing contour extraction methods. The result of tri-directional spotlight filter and adaptive spotlight filter method obtain the precision contour results, as shown in Figure 11(c) and 11(d), which is similar to the result of the proposed SAHLBSF method. One can also see the extracted contour of basicspotlight filter deviates from the real edge points, as shown in Figure 11 (b), whose result was affected by using asingle spotlight alone. The contour extraction result of Somkantha et al. method can beexamined by Figure 11(f), whose contour is slightly shifted to the left side and falls exactly on the edge.

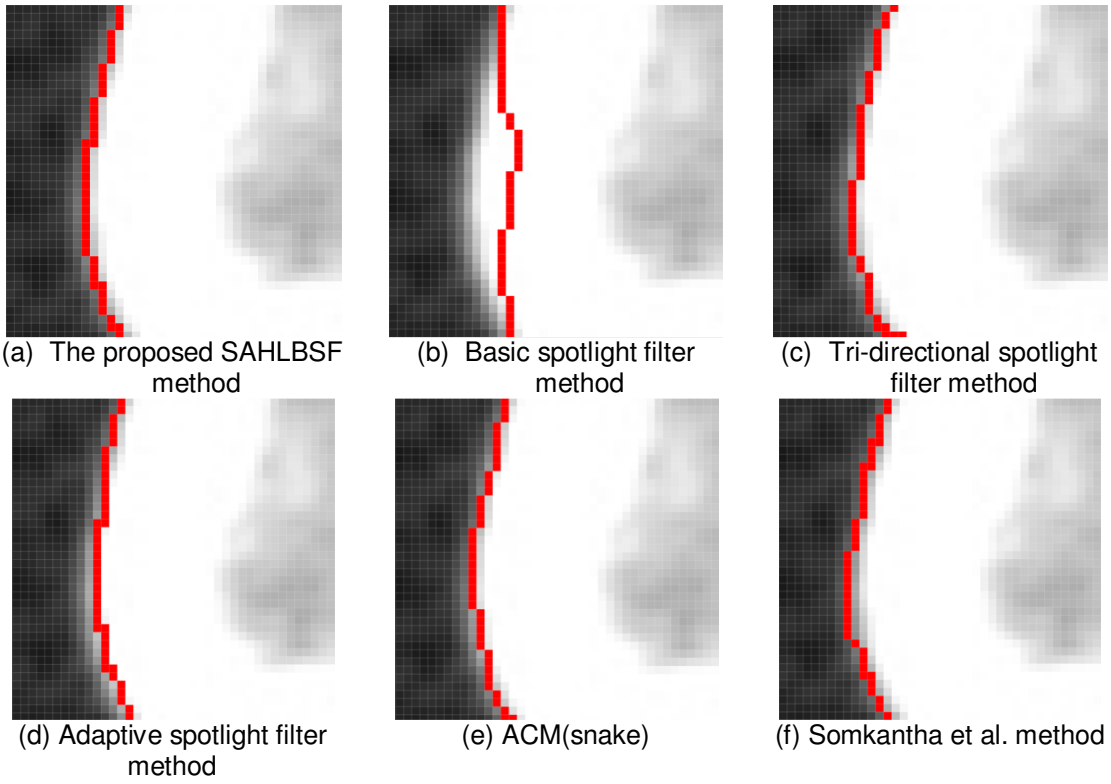

(a) The proposed SAHLBSF method (b) Basic spotlight filter method (c) Tri-directional spotlight filter method

(d) Adaptive spotlight filter method (e) ACM(snake) (f) Somkantha et al. method

FIGURE 11: Selected block of the same portion of contour from Figure 9 is magnified and shown for each comparing method.

In order to further show the accuracy of the contour extraction of the proposed SAHLBSF method, the selected ROI spine image in Figure 9(b)is used and the contour extraction results of the comparing methods are overlaid on the spine image as shown in Figure 12. Selected block of the same portion of contour from Figure 12 is magnified and shown for each comparing method in Figure 13.

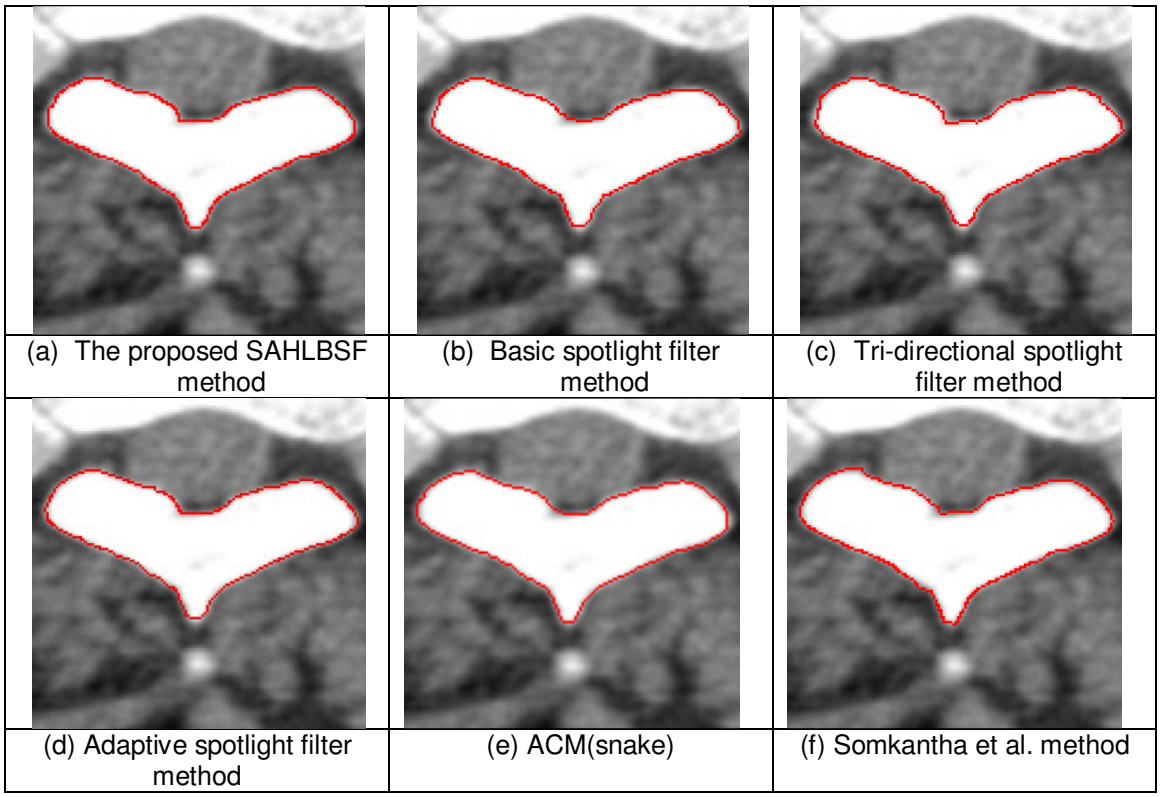

(a) The proposed SAHLBSF method | (b) Basic spotlight filter method | (c) Tri-directional spotlight filter method

(d) Adaptive spotlight filter method | (e) ACM(snake) | (f) Somkantha et al. method

FIGURE 12: The selected ROI spine image is used and the contour extraction results are shown.

For the spine image with sharp and long curvature, the proposed SAHLBSF method still achieve best contour extraction result in comparing with other methods, as can be seen in Figure 12(a) and Figure 13(a). The basic spotlight is insufficient to completely cover the long curvature portion of the contour such that the selection of continuous contour points is not precise and a series of error contour are generated as shown in Figure 12(b) and Figure 13(b). The contour extraction results of the tri-directional spotlight are shown in Figure12(c) and Figure13(c). Because the curvature contour areas are accurately covered by the three spotlight sectors, the aforementioned insufficient coverage problems of single basic spotlight filter can be avoided and a closed matching contour is obtained.

The contour extraction result of the adaptive spotlight filter is shown in Figure 12(d) and Figure 13(d).By visual inspecting of the results, one can found that the adaptive spotlight adaptively extends spanning angle for spotlight, which is suitable to accurately calculate local structure information for each curvature contour. The extraction results of snake are shown in Figure 12(e) and Figure 13(e), which shows good extraction result similar to that of the proposed SAHLBSF method. Figure 12(f) and Figure 13(f) show the results of Somkantha et al. method, where some misjudgment of the contour matching is generated in the upper concave block, and because the extraction relies on the result of the edge intensity map such that a grey area was not extracted. In conclusion, the proposed SAHLBSF method is obviously better than other existing contour extraction methods by the visual inspection, and the extracted contour is closer to the edge points of the object.

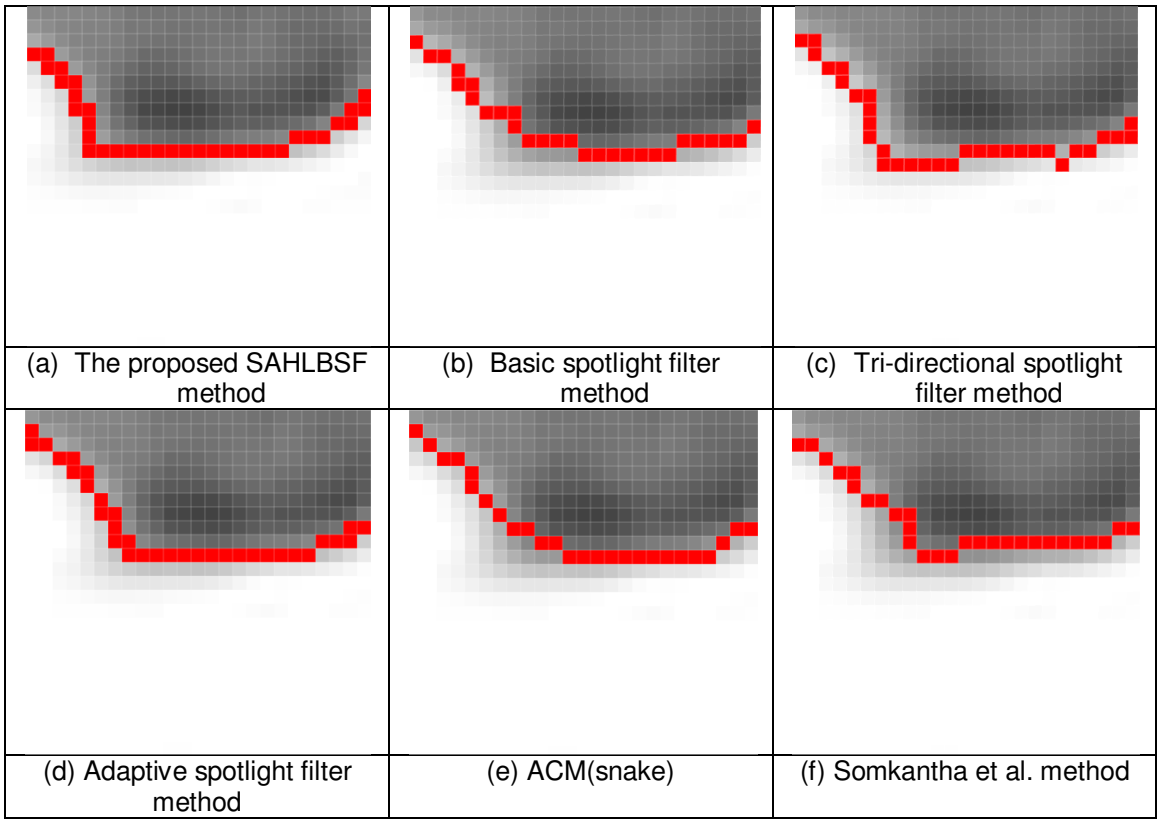

(a) The proposed SAHLBSF method | (b) Basic spotlight filter method | (c) Tri-directional spotlight filter method

(d) Adaptive spotlight filter method | (e) ACM(snake) | (f) Somkantha et al. method

FIGURE 13: Selected block of the same portion of contour from Figure 9 is magnified and shown for each comparing method.

5. CONCLUSION

Inspired bytheuser experience of driving a car, a self-adaptive high/low beam spotlight filter (SAHLBSF) in capturing local structure information for object contour extraction is proposed in this study. In searching the contour points in between pairs of initial contour points,the proposed SAHLBSF method is capable of adaptively determining whichspotlightto use by the local structure captured by the high beam and low beam spotlight sectoralong each pair of initial contour points. Once all pairs of initial contour points are processed by the SAHLBSF, the one-pixel width of object contour can then be obtained through the operation of filtering, dilation and thinning process fortheedge strength map. In the experimental results, the method in this paper is compared with other spotlight filter methods. Compared with the existing contour extraction of the active contour model (snake), the proposed method of this study does not require a large number of accurate initial points to achieve the contour extraction effect. Among the other spotlight filter methods, the proposed SAHLBSF method in this paper greatly improves the efficiency of the spotlight filtering operation. In terms of accuracy for artificial images, the proposed SAHLBSF methodof this study is superior to other existing methods. Therefore, in terms of computational efficiency and accuracy, the SAHLBSF method proposed in this study achieves a balance between the two requirements, andobtains the best contour extraction results among other existing methods.

6. REFERENCES

Bakir, H., & Charfi, M. (2009). Automatic medical image segmentation based on EPGV-snake, 2009 6th International Multi-Conference on System. Signals and Devices.

Barat, C., & Lagadec, B. (2008, March). A corner tracker snake approach to segment irregular object shape in video image. In 2008 IEEE International Conference on Acoustics, Speech and Signal Processing (pp. 717-720). IEEE.

Canny, J. (1986). A computational approach to edge detection. IEEE Transactions on pattern analysis and machine intelligence, (6), 679-698.

Chen, Q., Xue, B., Sun, Q., & Xia, D. (2010, September). Interactive image segmentation based on object contour feature image. In 2010 IEEE International Conference on Image Processing (pp. 3605-3608). IEEE.

Guo, Z., & Hall, R. W. (1989). Parallel thinning with two-subiteration algorithms. Communications of the ACM, 32(3), 359-373.

Hamed Mozaffari, M., & Lee, W. S. (2019). Domain adaptation for ultrasound tongue contour extraction using transfer learning: A deep learning approach. The Journal of the Acoustical Society of America, 146(5), EL431-EL437.

Hojjatoleslami, S. A., & Kittler, J. (1998). Region growing: a new approach. IEEE Transactions on Image processing, 7(7), 1079-1084.

Hsu, R. C., Chan, D. Y., Lai, W. C., & Liu, C. T. (2011, November). An improved automatic initial snaxel selection with corner tracing for object contour extraction in medical image. In 2011 Visual Communications and Image Processing (VCIP) (pp. 1-4). IEEE.

Hsu, R. C., Hsu, C. H., Liu, C. T., & Qiu, G. H. (2014, July). A tri-directional spotlight filter for object contour extraction. In 2014 International Conference on Audio, Language and Image Processing (pp. 516-520). IEEE.

Jaumard-Hakoun, A., Xu, K., Roussel-Ragot, P., Dreyfus, G., &Denby, B. (2016). Tongue contour extraction from ultrasound images based on deep neural network. arXiv preprint arXiv:1605.05912.

Kass, M., Witkin, A., & Terzopoulos, D. (1988). Snakes: Active contour models. International journal of computer vision, 1(4), 321-331.

Lin, C. C. (2013, July) Object Contour Extraction Using local structure information captured by Spotlight Filter. Master thesis, National Chiayi University, Taiwan.

Liu, C. T., Lin, C. C., & Hsu, R. C. (2012, March). An object contour extraction using local structure information captured by a spotlight filter. In 2012 IEEE International Conference on Acoustics, Speech and Signal Processing (ICASSP) (pp. 1177-1180). IEEE.

Liu, L., & Sclaroff, S. (2004). Deformable model-guided region split and merge of image regions. Image and Vision Computing, 22(4), 343-354.

Qiao, Y., Truman, M., & Sukkarieh, S. (2019). Cattle segmentation and contour extraction based on Mask R-CNN for precision livestock farming. Computers and Electronics in Agriculture, 165, 104958.

Ruhaiyem, N. I. R., & Hammade, N. A. (2021). Cerebrovascular Segmentation Based on Edge Preserving Filters Technique in Magnetic Resonance Angiography Images: A Systematic Review. International Journal of Image Processing, (pp. 48-67), 15(4).

Somkantha K.,Theera-Umpon N., and Auephanwiriyakul S. (2011).Boundary Detection in Medical Images Using Edge Following Algorithm Based on Intensity Gradient and Texture Gradient Features. IEEE Transactions on Biomedical Engineering, 58(3), (pp.567-573).

Suzuki, K., Horiba, I., Sugie, N., &Nanki, M. (2004). Extraction of left ventricular contours from left ventriculograms by means of a neural edge detector. IEEE Transactions on Medical Imaging, 23(3), 330-339.

Talukder, M. H., Ogiya, M., Takanokura, M. (2018). New Noise Reduction Technique for Medical Ultrasound Imaging using Gabor Filtering. International Journal of Image Processing, (pp. 28-38), 12(1).

Weimer, D., Scholz-Reiter, B., & Shpitalni, M. (2016). Design of deep convolutional neural network architectures for automated feature extraction in industrial inspection. CIRP annals, 65(1), 417-420.

Xu, K., GáborCsapó, T., Roussel, P., & Denby, B. (2016). A comparative study on the contour tracking algorithms in ultrasound tongue images with automatic re-initialization. The Journal of the Acoustical Society of America, 139(5), EL154-EL160.

Yan, P., & Kassim, A. A. (2006). Medical image segmentation using minimal path deformable models with implicit shape priors. IEEE Transactions on Information Technology in Biomedicine, 10(4), 677-684..

Yang, W., Cai, J., Zheng, J., & Luo, J. (2010). User-friendly interactive image segmentation through unified combinatorial user inputs. IEEE Transactions on Image Processing, 19(9), 2470-2479.

Zhang, M., Liu, X., Xu, D., Cao, Z., & Yu, J. (2019). Vision-based target-following guider for mobile robot. IEEE Transactions on Industrial Electronics, 66(12), 9360-9371.

Zhang, D., Yang, M., Tao, J., Wang, Y., Liu, B., & Bukhari, D. (2016, March). Extraction of tongue contour in real-time magnetic resonance imaging sequences. In 2016 IEEE International Conference on Acoustics, Speech and Signal Processing (ICASSP) (pp. 937-941). IEEE.

Zhu, J., Styler, W., & Calloway, I. (2019). A CNN-based tool for automatic tongue contour tracking in ultrasound images. arXiv preprint arXiv:1907.10210.